# UC Irvine
## UC Irvine Previously Published Works

**Title**

Convective beam ion losses due to Alfvén eigenmodes in DIII-D reversed-shear plasmas

**Permalink**

**Journal**

**ISSN**

**Authors**

Pace, DC
Fisher, RK
García-Muñoz, M
et al.

**Publication Date**

**DOI**

**Copyright Information**

Peer reviewed

## BRIEF COMMUNICATION

# Convective beam ion losses due to Alfvén eigenmodes in DIII-D reversed-shear plasmas

**D C Pace**[1]**, R K Fisher**[2]**, M García-Muñoz**[3]**, W W Heidbrink**[1] **and M A Van Zeeland**[2]

[1] Department of Physics and Astronomy, University of California-Irvine, Irvine, CA 92697, USA
[2] General Atomics, PO Box 85608, San Diego, CA 92186-5608, USA
[3] Max-Planck Institut für Plasmaphysik, Garching D-85748, Germany

E-mail: pacedc@fusion.gat.com

### Abstract

Coherent losses of neutral beam ions are observed at frequencies corresponding to toroidal and reversed-shear Alfvén eigenmodes (RSAEs) in DIII-D. Reversed-shear profiles are created by injecting beam power during the plasma current ramp. Beam ion losses stemming from Alfvén eigenmode activity contribute to flattening of the energetic ion density profile in such discharges. This is the first observation of convective beam ion losses due to RSAEs. The energies and pitch angles of lost ions are measured and found to exist within a well-defined region of phase space. Loss flux signals decrease in time as current penetrates and Alfvén eigenmode activity becomes more core localized. Preliminary Monte Carlo simulations of energetic ion interactions with measured mode structures show the dominant loss mechanism is a transition from a counter-passing orbit to a trapped orbit that is lost to the wall.

(Some figures in this article are in colour only in the electronic version)

## 1. Introduction

Energetic ion transport is an active area of interest for magnetically confined fusion research with particular relevance to ITER [1]. Fusion produced alpha particles will excite a spectrum of Alfvén eigenmodes (AEs) [2] in ITER that may, in turn, affect alpha confinement on time scales shorter than a slowing-down time. The resulting increase in alpha transport may reduce the self-heating ability of reactors, which would also reduce net energy gain.

Energetic ions are capable of experiencing radial transport from interactions with toroidal Alfvén eigenmodes (TAEs) [3, 4] and reversed-shear Alfvén eigenmodes (RSAEs) [5, 6]. In experiments, energetic ion sources include neutral beam injection and ion cyclotron resonance

heating (ICRH). The first TAE experiments inferred losses of beam ions from drops in neutron emission [7, 8]. Measurements of direct losses to the walls were obtained shortly thereafter [9, 10]. Losses of ICRH tail ions due to TAEs were first measured by a neutral-particle analyzer [11] and by a poloidal array of scintillators [12]; the latter work also studied beam ion losses. More recently, coherent oscillations of escaping ICRH tail ions at TAE frequencies have been observed [13]. For RSAEs, suppressed neutron rates during neutral beam injection correlate with mode activity [14, 15]. Coherent oscillations of escaping ICRH tail ions at RSAE frequencies have also been observed [16]. In plasmas that produced RSAEs using neutral beam injection only, however, no coherent beam ion losses at RSAE frequencies were observed [17]. That work found RSAEs contributed to beam ion redistribution in the core and likely increased the ability of TAEs to produce direct losses.

A series of experiments investigating AE-induced transport of neutral beam injected ions has been conducted on the DIII-D tokamak [18, 19]. The core energetic ion density profile is observed to flatten in the presence of AE activity [20, 21]. A new fast ion loss detector (FILD) [22] has since been commissioned to measure the energy and pitch angle of energetic ions lost to its position on the wall. In reversed-shear plasmas similar to those of the earlier experiments, FILD measurements demonstrate losses at TAE and RSAE frequencies. This result helps us to explain the previously observed energetic ion profile flattening. Furthermore, these results represent the first direct measurement of beam ion losses at RSAE frequencies.

The organization of this paper is as follows. In section 2 the experimental setup and diagnostics are presented. Focus is placed on the energy and pitch angle measurement of beam ions reaching a detector at the wall. Section 3 presents the observations of beam ion losses coherent with Alfvénic activity. Conclusions are presented in section 4, where implications for future energetic ion transport studies are discussed.

## 2. Diagnostics and plasma parameters

The energetic ion population in DIII-D (typical parameters of $B_T = 2.1$ T, $R = 1.66$ m and $a = 0.67$ m) is produced by neutral beam injection from up to eight sources providing 2.5 MW injected power each. The geometry of these beams is shown in figure 1. The beams are located at four different toroidal positions ($\phi = 30°, 150°, 210°$ and $330°$), with each unit housing a tangential (tangency radius $R_{tan} = 1.15$ m) and a perpendicular ($R_{tan} = 0.74$ m) injection line. Injection paths corresponding to each source are labeled in the figure according to whether they are the left or right source in the housing. The firing pattern of these beams determines the instantaneous pitch angle range ($\chi = v_{\parallel}/v$) of the energetic ion distribution. Additional variability is available from the 210° beam that injects counter to the standard plasma current direction shown in figure 1 ($\chi < 0$). The behavior and confinement of the beams is well understood experimentally [23] and is modeled by the NUBEAM [24, 25] module of TRANSP [26] to calculate heating and other parameters of interest.

A collection of diagnostics used in this research is also shown in figure 1. Radial profiles of energetic ion density and information concerning the distribution is measured by the vertical fast ion $D_{\alpha}$ (FIDA) [27] system that views the 330°-L neutral beam. This diagnostic measures Doppler shifted light emitted by energetic ions that charge exchange with beam injected neutrals. A neutron detection system [28] located at $\phi = 105°$ just outside of the vacuum vessel measures 2.45 MeV neutrons produced by DD fusion. While the FIDA and neutron diagnostics measure parameters related to the core confinement of beam ions, the scintillator based FILD measures energetic ion fluxes reaching its position on the wall as a function of pitch angle and energy. The scintillator is covered by a graphite head with a collimating aperture. Ions passing through the aperture strike the scintillator at a position determined
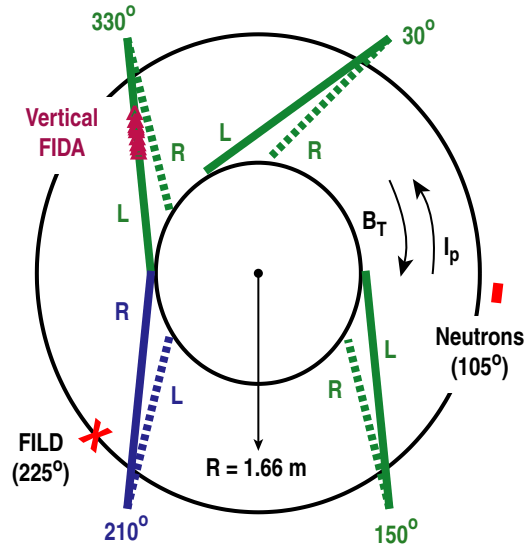
**Figure 1.** Schematic top view of DIII-D indicating neutral beam geometry and diagnostic positions in terms of toroidal position, $\phi$. The FILD is indicated by the 'X' at $\phi = 225°$ and the neutron detector by a rectangle at $\phi = 105°$. The vertical FIDA system views are marked by triangles at the viewing chord intersections with the $330°$-L neutral beam. Directions for the toroidal magnetic field, $B_T$, and plasma current, $I_p$, for the discharges discussed here are shown.

according to their energy (gyroradius) and pitch angle. Scintillator light passes through an optical train and out of the probe shaft where it is split between a slow charge-coupled device (CCD) camera sampled at 160 Hz and a fast photomultiplier tube (PMT) sampled at 1 MHz. Figure 2 demonstrates the important features of the FILD. Figure 2(a) displays the poloidal cross-section from shot 142111 ($B_T = 2.05$ T, $R = 1.71$ m, $a = 0.62$ m, inner wall limited) at $t = 570$ ms. The FILD is located at a position approximately $45°$ below the outer midplane and the aperture is marked in figure 2 by the $\times$ at $[R, z] = [2.2, -0.7]$ m. Full orbit paths for ions of pitch angle $\alpha = \cos^{-1}(\chi) = 35°, 55°$ and $75°$ are plotted. All three ion orbits are detectable by the FILD and feature energy $E = 80$ keV. In figure 2(b) a schematic of the FILD highlights important operational features. An example ion orbit is shown passing through the aperture and striking the scintillator surface. The wide opening in the figure is the cutout of the graphite shield, while the collimating aperture is an Inconel slit inside of this shield that is <1 mm wide in the direction that resolves the gyroradius. Figure 2(c) is a partially three-dimensional view of a narrow region near the probe head. The FILD graphite head is labeled and the orbits from figure 2(a) intersect at the position of the aperture (which is drawn oversize for clarity). The FILD features a linear translator that allows adjustment of its radial position. The edge of the graphite head is typically placed more than 10 cm away from the last closed flux surface to minimize heat load that may lead to carbon impurity contributions.

In the results presented here, AEs are excited by neutral beam injection during the plasma current ramp [29]. Figure 3 displays the evolution of plasma parameters in shot 142111. A total of 7.1 MW of neutral beam power is injected during the current ramp as shown in figure 3(a). Electron density is plotted in figure 3(b), where it is observed to rise quickly when neutral beam injection begins. Indicators of energetic ion confinement are shown in figure 3(c). The FIDA density points are proportional to the energetic ion density [30] along the viewing chord at $R = 1.80$ m. The neutron rate is dominated by the beam-plasma production term
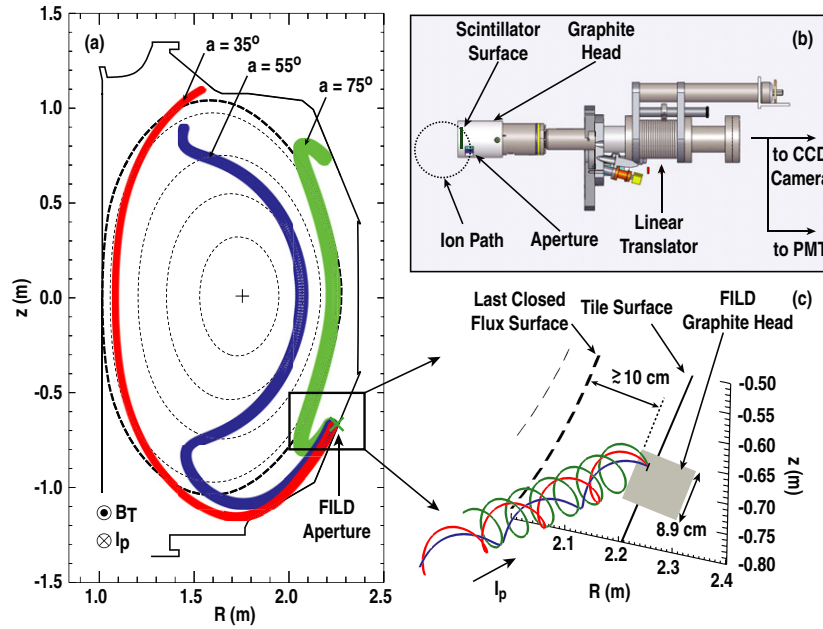
**Figure 2.** FILD Diagnostic: (*a*) poloidal cross-section of shot 142111 at $t = 570$ ms. The position of the FILD aperture is indicated by the $\times$ at $[R, z] = [2.25, -0.67]$ m. Three ion orbits, with $E = 80$ keV and $\alpha = \cos^{-1}(\chi) = 35°$, $55°$ and $75°$, that are detectable by the FILD are also shown. (*b*) Schematic of the FILD. (*c*) Zoomed in region of the plasma cross-section showing typical geometry during FILD operation.

and therefore represents beam ion confinement. In figure 3(*c*) these data are normalized to the classically expected values from TRANSP as developed in [20]. Both parameters are observed at values well below the expectation from classical transport alone, indicating the presence of an additional energetic ion transport mechanism.

## 3. Observed beam ion losses

A false color FILD camera frame from shot 142111 at $t = 525$ ms is shown in figure 4 labeling two regions of measured losses. Energetic ion losses measured by the FILD during this experiment include contributions from the convectively driven flux due to Alfvén eigenmodes and also from neutral beam prompt losses. Beam prompt losses occur when an injected neutral ionizes such that its first complete poloidal transit intersects the wall. Figure 4 shows prompt losses over the pitch angle range $60° \leqslant \alpha \leqslant 75°(\pm 5°)$. The uncertainty in pitch angle is a combination of the intrinsic resolution of the diagnostic as calculated by the Monte Carlo strike map code EfipDesign [31], and an additional contribution due to vibration of the initially installed optics platform. The three individual 'spots' of loss within this pitch angle range are centered on $r_L = 3.5$, 2.3 and 1.7 cm and correspond to the full, one-half and one-third energy injection of the $210°$-L source beam, respectively. Prompt losses are used to validate FILD operation and are modeled considering the three-dimensional geometry between the beams and the diagnostic [32].

By adjusting the zoom lens that focuses scintillator light onto the PMT-connected fiber optic it is possible to focus the PMT view onto a narrower region of the scintillator. During
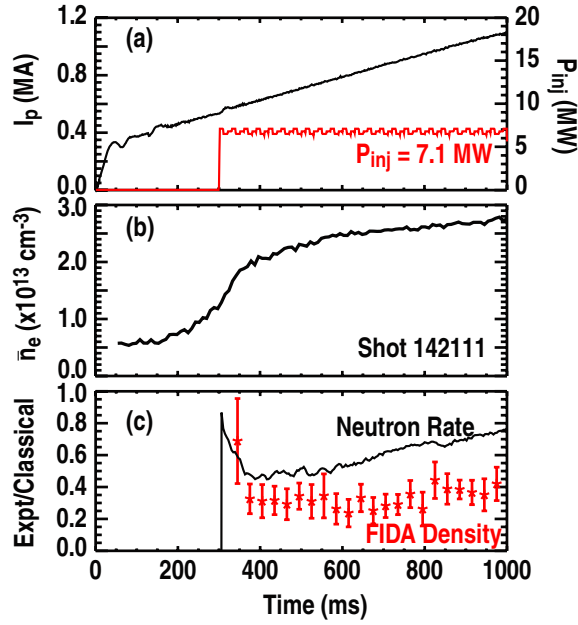
**Figure 3.** (*a*) Plasma current ramp ($I_p$, left axis) and injected neutral beam power ($P_{inj}$, right axis). (*b*) Line-averaged electron density. (*c*) Neutron rate (solid line) and FIDA density (data points) normalized to classical values. The FIDA density is measured at $R = 1.80$ m.
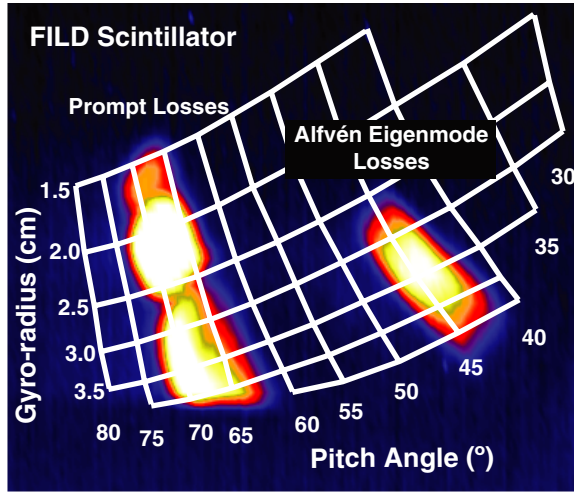


**Figure 4.** Camera frame from the FILD in shot 142111 at $t = 525$ ms. A grid indicating the gyroradius, $r_L$, and pitch angle of the impacting ions is plotted in white. The phase space of ions confirmed to be lost due to Alfvén eigenmode activity occurs between $2.7 \leqslant r_L \leqslant 4.5$ cm and $42° \leqslant \alpha \leqslant 47°$.

shot 142111 the PMT view is focused onto a region dominated by light from $40° \leqslant \alpha \leqslant 50°$. The wings of this view do incorporate some light from the region where $\alpha > 60°$. Figure 5(*a*) displays neutral beam power reaching the limiters, $P_{nb,lim}$, which is a measure of prompt losses as calculated by TRANSP. The prompt loss flux is reduced as the plasma current rises
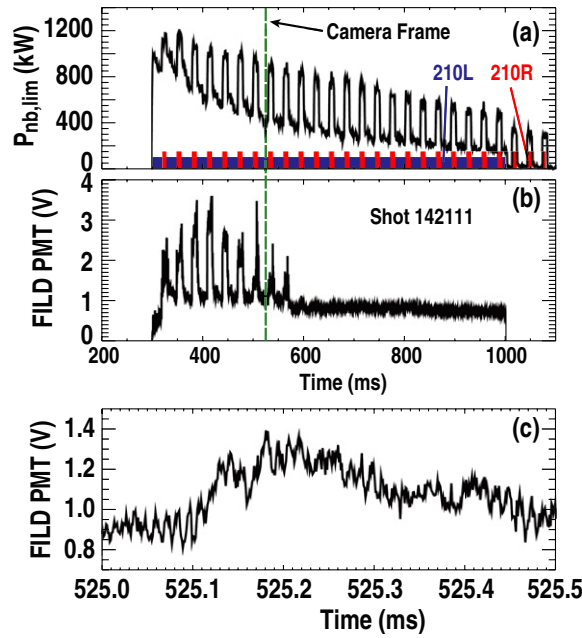
**Figure 5.** (*a*) Neutral beam power reaching the limiter, $P_{\text{nb,lim}}$, as computed by TRANSP. The firing patterns from the 210°-L (on constantly across $300 \leqslant t \leqslant 1000$ ms) and 210°-R neutral beams are shown. A dashed vertical line labeled 'Camera Frame' indicates the exposure of the CCD camera. (*b*) Smoothed signal from the FILD PMT during the current ramp. (*c*) Raw signal from the FILD PMT across a time region corresponding to the exposure of the CCD camera as shown in figure 4.

and banana orbit widths decrease. The firing patterns of the counter-injected neutral beams that produce FILD-observed prompt losses are indicated by rectangles below the $P_{\text{nb,lim}}$ trace. The 210°-L beam is on continuously from $300 \leqslant t \leqslant 1000$ ms (solid rectangle) while the 210°-R beam fires in 10 ms wide pulses represented by the slender rectangles. The FILD PMT signal during this time is shown in figure 5(*b*). Over this wide time range only large scale changes due to prompt losses are discernible. The 210°-L produces a slowly varying loss (signal level $\approx 1$ V in figure 5(*b*)). Orbit modeling shows that the prompt loss contribution from the 210°-R beam reaches the FILD in the 40°–50° pitch angle range at low plasma current and moves closer to the midplane (where it is no longer detectable by the FILD) as the current increases. For early times, modulation of the PMT signal is dominated by pulses of the 210°-R beam. This behavior confirms the expected viewing range set by the PMT zoom lens. The vertical dashed line of figures 5(*a*) and (*b*) marks the camera exposure of figure 4 showing that the 210°-R beam is off and prompt losses do not contribute to the $40° \leqslant \alpha \leqslant 50°$ loss region.

The region of losses shown in figure 4 occurring over $40° \leqslant \alpha \leqslant 50°$ is identified as losses due to AEs. The raw PMT trace acquired over the exposure time of the camera frame is plotted in figure 5(*c*). Coherent oscillations with a period of $T \approx 12$–$17\,\mu$s ($f \approx 60$–$85$ kHz) are observed (perhaps most clearly near $t = 525.1$ ms) and found to be consistent with AE frequencies. These losses occur at $r_{\text{L}} \approx 3.5$ cm, corresponding to ions of $E \approx 75$ keV given the amplitude of the magnetic field at the FILD, $B_{\text{FILD}} = 1.5$ T. The exposure time of the camera is $500\,\mu$s, which is short enough that a nearly constant set of AE frequencies is observed.

Power spectra demonstrating the presence of Alfvén eigenmodes and coherent energetic ion losses are shown in figure 6. Figure 6(*a*) displays the cross power between a line-integrated
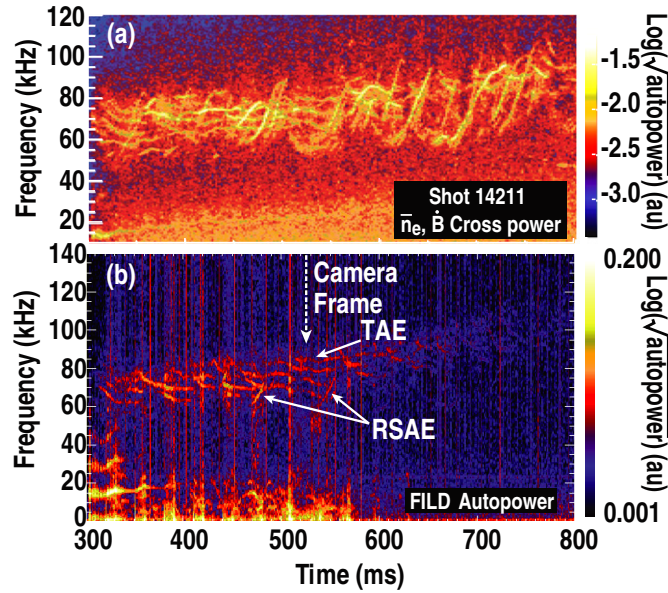
**Figure 6.** (*a*) Spectrogram of cross power between a line-averaged electron density measurement ($\bar{n}_e$) and a magnetic coil ($\dot{B}$). (*b*) Spectrogram of autopower from a PMT viewing the Alfvén eigenmode loss region of the FILD scintillator. Example TAE and RSAE activity bands are highlighted. A dashed vertical arrow is placed at $t = 525$ ms to indicate the time at which the frame of figure 4 is acquired.

electron density measurement from a laser interferometer [33] and a $\dot{B}$-coil [34]. The activity occurring between approximately 50 and 100 kHz is a collection of toroidal and RSAEs. Figure 6(*b*) is an autopower spectrogram from the FILD PMT demonstrating coherent losses in the RSAE and TAE frequency ranges. The dashed vertical arrow marks the time slice of the FILD camera frame in figure 4. The FILD spectrum shows that loss activity decreases steadily in time and is nearly zero by $t = 800$ ms. Figure 6(*a*) further shows that the core Alfvén eigenmode spectrum transitions from mostly TAEs at early times to nearly all RSAEs after 600 ms. The AE activity is becoming more core localized as plasma current increases, while particle loss boundaries are moving outward, thereby reducing the ability of AEs to place beam ions directly onto loss orbits (i.e. convective losses decrease [16]). Loss boundaries at $t \approx 525$ ms and $t \approx 725$ ms for ions of 80 keV energy in shot 142111 are shown in figures 7(*a*) and (*b*), respectively. These phase space contours describe orbits as a function of major radius position along the outer midplane. A dashed white line marks the innermost position for which loss orbits exist. During the earlier time shown in figure 7(*a*), the position of $q_{min}$ (a proxy for AE location) is further out than the loss boundary and it is expected that convective AE-induced losses are more easily produced. For the later time shown in figure 7(*b*), $q_{min}$ is inside of the loss boundary and convective losses are expected to decrease.

In addition to the Alfvén-induced loss activity above 60 kHz, the FILD spectrogram of figure 6(*b*) also displays coherent activity at lower frequencies. Prior to $t = 400$ ms there are losses at $f \approx 15$ kHz, and a second and third harmonic, that are coherent with an observed energetic particle induced geodesic acoustic mode (EGAM) [35, 36]. The ion/EGAM interaction that leads to these losses is presently under investigation. Other apparent bursts of low frequency losses that extend down to zero frequency (e.g. appearing just before and after
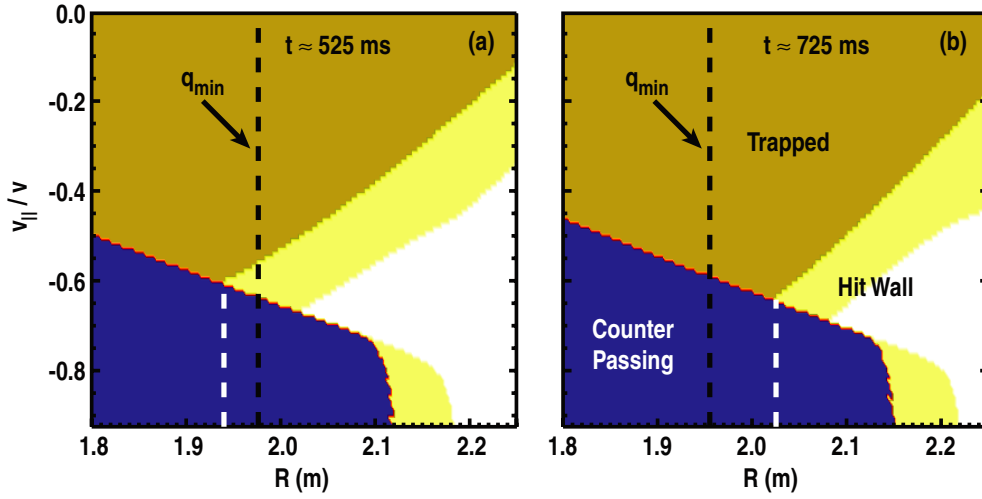
**Figure 7.** Orbit phase space for ions of energy $E = 80\,keV$ on the midplane in shot 142111 at (a) $t \approx 525\,ms$ and (b) $t \approx 725\,ms$. Regions of trapped, counter-passing, and wall striking orbits are labeled in (b). The dashed black line in each panel indicates the position of $q_{min}$ and the white dashed line represents the innermost major radius position for which loss orbits exist.

$t = 400\,ms$) are artifacts due to the square-wave like prompt loss flux from individual pulses of the $210°$-R beam.

Spectrograms from a narrow time region, $450 \leqslant t \leqslant 520\,ms$, when the RSAE losses are prominent, are shown in figure 8. The FILD spectrum of figure 8(a) displays the largest fluctuations due to RSAE losses in a 60–70 kHz band passing through 480 ms. The contour lines overlaid on this FILD spectrogram represent a single level from the interferometer phase spectrogram shown in figure 8(b). This interferometer data comes from a single chord passing through the plasma along the horizontal midplane. While there is little sign of TAEs in the interferometer spectra, these modes do still appear in the FILD spectra (e.g. the three nearly constant frequency features at 500 ms). A comparison between panels 8(a) and (b) shows that there are many instances in which an RSAE identified in the interferometer data does not produce FILD measured beam ion losses. It remains to be determined whether losses are being produced in another region of phase space for which there is no PMT view, or whether such losses may simply reach a different position on the outer wall of vessel. Future work adding more PMT views addresses the first point, while a new FILD installed just below the outer midplane will address the second.

A preliminary investigation of the interaction between beam ions and the excited AEs is conducted by way of simulation. The plasma equilibrium and Alfvén wave fields are provided as input to the Hamiltonian guiding center code ORBIT [37], which then calculates the resulting path of beam ions due to these modes. The full poloidal structure of the wave fields is calculated by NOVA-K [38] using the radial eigenmode profile from temperature fluctuations measured by an electron cyclotron emission diagnostic [39]. Resonance between the ions and the modes is achieved when [2, 40] $\omega = n\omega_\phi - (m + l)\omega_\theta$, where $\omega$ is the Alfvén eigenmode frequency, $n$ ($m$) is the toroidal (poloidal) mode number, $l$ is a quantum number and $\omega_\phi$ ($\omega_\theta$) is the ion's toroidal (poloidal) precession frequency. The simulation employs a Monte Carlo method in which a number of beam injected particles are tracked. Each ion's initial properties (e.g. deposition position, energy, and pitch angle) are determined from NUBEAM
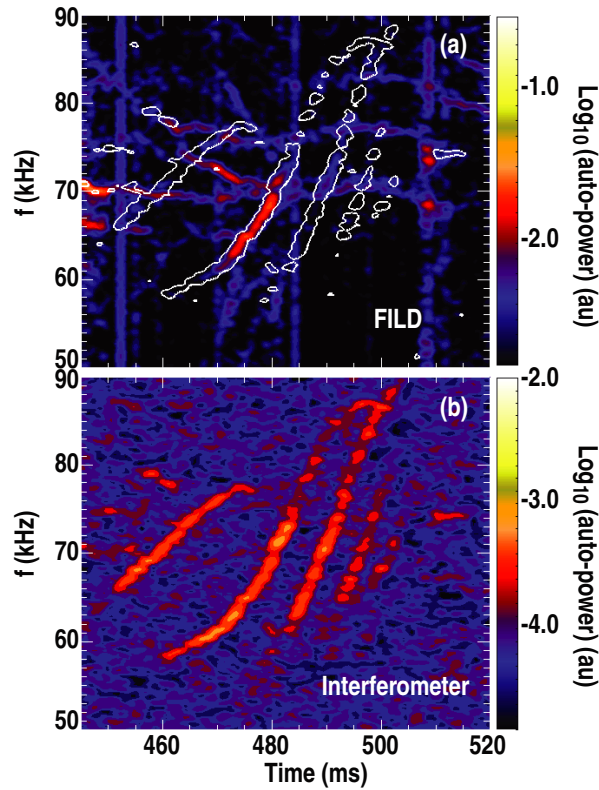
**Figure 8.** (*a*) Spectrogram of FILD PMT signal from shot 142111 over a narrow time region corresponding to coherent RSAE losses (color contour). The overlaid contour lines represent the $-3.67$ contour level of the interferometer phase spectrogram that is plotted in panel (*b*).

modeling. The coordinate system in ORBIT is defined by flux surfaces and does not extend beyond the separatrix, meaning that simulated ions are defined to be lost when they reach the separatrix. This class of particles does not necessarily represent ions that are lost to the wall. To extend the applicability of ORBIT simulations to losses, a gyrocenter orbit code that works in real space has been incorporated. The implementation takes the properties of ORBIT ions at the position where they intersect the separatrix and uses that information to compute a gyrocenter orbit across a full poloidal transit. If this ion trajectory intersects the wall, then the ion is recorded as lost.

Figure 9 presents an example of the simulation result. The solid line is an ORBIT calculated gyrocenter trajectory of an ion with $E = 75\,\text{keV}$ and $\chi = 0.66$ (pitch at the FILD, though the ion begins on a counter-current passing orbit) as simulated by ORBIT in the presence of a spectrum of AEs. The total time elapsed along this trajectory is $\Delta t < 400\,\mu\text{s}$, demonstrating that the transport process may be studied in a fixed equilibrium. Interaction between the ion and the AEs results primarily in the reduction in the ion's toroidal canonical momentum ($\delta P_\phi / P_\phi \approx 14\%$). Ion energy changes much less ($\delta E / E \approx 2\%$), which is expected since the observed losses occur at energies corresponding to the full neutral beam energy. The dashed line connecting to the ORBIT evolved path represents the separately calculated wall-strike path using the properties of the ion at its intersection with the separatrix. This part of the trajectory intersects a small rectangle encompassing the FILD aperture ($\times$). The rectangle
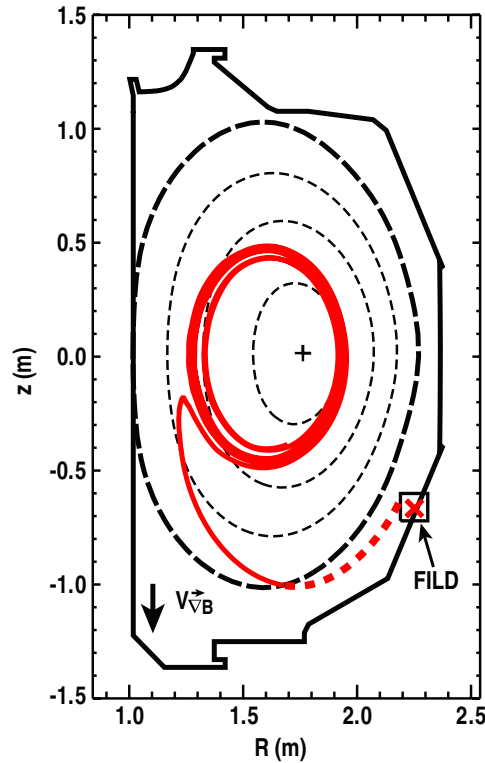
9

**Figure 9.** Simulated ion trajectory (solid line) as identified by ORBIT in the magnetic equilibrium of shot 142111 at $t = 525$ ms. The dashed line connecting to the ORBIT evolved trajectory represents the separately calculated wall-strike path. The FILD aperture is indicated by the $\times$ and the black rectangle surrounding this aperture represents the FILD region that is used to define a measured lost ion in the ORBIT simulations.

defines the simulated FILD region: any ion that passes through this region is considered a FILD-detectable ion. The properties of this simulated ion are consistent with FILD measurements. Details of this work and the comparison between measured and simulated losses are given in [41].

## 4. Conclusion

In summary, convective losses of beam ions due to Alfvén eigenmode activity have been measured with a scintillator detector in reversed-shear DIII-D plasmas. These observations indicate the AE-induced losses likely contributed to the previously observed flattening of the energetic ion density profile [20, 21]. The first observations of beam ion losses coherent with RSAEs are also presented. Other experiments have shown that ICRH tail ions can be directly expelled by RSAEs [16], and that energetic ion losses increase in situations where RSAE existence regions overlap with TAE regions [14, 16]. The present results demonstrate that the energetic ion distribution produced in ICRH plasmas is not a requirement to satisfy the relevant resonance condition for convective RSAE losses. One suggestion to reduce RSAE-influenced losses is to operate with equilibria that place $q_{\min}$ outside the range in which RSAEs are able to transition to TAEs [14]. The results presented here suggest that a general emphasis should

be placed on keeping $q_{min}$ and AE radial extent inside of the energetic ion loss boundary. Simulation of beam ion interactions with a spectrum of AEs illustrates a possible trajectory evolution from a confined passing ion to a FILD-detectable loss on a large banana orbit. Future work should perform simulations using a larger number of Monte Carlo particles with the aim of providing adequate statistics in the perturbation field of a single RSAE. Given that RSAEs can be excited due to the equilibrium perturbation of sawtooth crashes [42], it is important to consider that they may be capable of contributing to the energetic ion transport observed in sawtoothing plasmas [43, 44]. Ongoing investigations of sawtooth-induced transport [45, 46] will be able to incorporate energetic ion loss measurements and core transport measurements simultaneously.

## Acknowledgments

## References

[1]  Fasoli A *et al* 2007 *Nucl. Fusion* **47** S264
[2]  Heidbrink W W 2008 *Phys. Plasmas* **15** 055501
[3]  Cheng C Z and Chance M S 1986 *Phys. Fluids* **29** 3695
[4]  Cheng C Z, Chen L and Chance M S 1985 *Ann. Phys.* **161** 21
[5]  Berk H L *et al* 2001 *Phys. Rev. Lett.* **87** 185002
[6]  Sharapov S E *et al* 2002 *Phys. Plasmas* **9** 2027
[7]  Wong K L *et al* 1991 *Phys. Rev. Lett.* **66** 1874
[8]  Heidbrink W W *et al* 1991 *Nucl. Fusion* **31** 1635
[9]  Duong H H *et al* 1993 *Nucl. Fusion* **33** 749
[10]  Darrow D S *et al* 1992 *Proc. 19th European Conf. on Plasma Physics and Controlled Fusion (Innsbruck, Austria)*
[11]  Ali-Arshad S and Campbell D J 1995 *Plasma Phys. Control. Fusion* **37** 715
[12]  Darrow D S *et al* 1997 *Nucl. Fusion* **37** 939
[13]  García-Muñoz M *et al* 2008 *Phys. Rev. Lett.* **100** 055005
[14]  Takechi M *et al* 2005 *Phys. Plasmas* **12** 082509
[15]  Van Zeeland M A *et al* 2008 *Plasma Phys. Control. Fusion* **50** 035009
[16]  García-Muñoz M *et al* 2010 *Phys. Rev. Lett.* **104** 185002
[17]  García-Muñoz M *et al* 2010 *Proc. 23rd IAEA Fusion Energy Conference (Daejon, Korea)* EXW/P7-07
[18]  Luxon J L 2002 *Nucl. Fusion* **42** 614
[19]  Strait E J 2009 *Nucl. Fusion* **49** 104008
[20]  Heidbrink W W *et al* 2007 *Phys. Rev. Lett.* **99** 245002
[21]  Heidbrink W W *et al* 2008 *Nucl. Fusion* **48** 084001
[22]  Fisher R K *et al* 2010 *Rev. Sci. Instrum.* **81** 10D307
[23]  Heidbrink W W *et al* 2009 *Plasma Phys. Control. Fusion* **51** 125001
[24]  Goldston R J *et al* 1981 *J. Comput. Phys.* **43** 61
[25]  Pankin A *et al* 2004 *Comput. Phys. Commun.* **159** 157
[26]  See http://w3.pppl.gov/transp, the official homepage of TRANSP, for information concerning the models and methods employed, in addition to usage documentation
[27]  Luo Y *et al* 2007 *Rev. Sci. Instrum.* **78** 033505
[28]  Heidbrink W W, Taylor P L and Phillips J A 1997 *Rev. Sci. Instrum.* **68** 536
[29]  Van Zeeland M A *et al* 2006 *Phys. Rev. Lett.* **97** 135001
[30]  Heidbrink W W *et al* 2004 *Plasma Phys. Control. Fusion* **46** 1855
[31]  Werner A *et al* 2001 *Rev. Sci. Instrum.* **72** 780
[32]  Pace D C *et al* 2010 *Rev. Sci. Instrum.* **81** 10D305

[33] Van Zeeland M A *et al* 2006 *Rev. Sci. Instrum.* **77** 10F325
[34] Strait E J 2006 *Rev. Sci. Instrum.* **77** 023502
[35] Nazikian R *et al* 2008 *Phys. Rev. Lett.* **101** 185001
[36] Fu G Y 2008 *Phys. Rev. Lett.* **101** 185002
[37] White R B and Chance M S 1984 *Phys. Fluids* **27** 2455
[38] Cheng C Z 1992 *Phys. Rep.* **211** 1
[39] Austin M E and Lohr J 2003 *Rev. Sci. Instrum.* **74** 1457
[40] Todo Y and Sato T 1998 *Phys. Plasmas* **5** 1321
[41] Van Zeeland M A *et al* 2011 Measurements and modeling of Alfvén eigenmode induced fast ion transport and loss in DIII-D and ASDEX Upgrade *Phys. Plasmas* at press
[42] Edlund E M *et al* 2009 *Phys. Rev. Lett.* **102** 165003
[43] Sadler G J *et al* 1990 *Fusion Technol.* **18** 556
[44] Fisher R K *et al* 1995 *Phys. Rev. Lett.* **75** 846
[45] Nielsen S K *et al* 2010 *Plasma Phys. Control. Fusion* **52** 092001
[46] Van Zeeland M A *et al* 2010 *Nucl. Fusion* **50** 084002